Journal of Materials Science: Materials in Electronics (2018) 29:16702–16714
https://doi.org/10.1007/s10854-018-9763-z

Synthesis, characterization and optical properties of multi-walled carbon nanotubes/aniline-*o*-anthranilic acid copolymer nanocomposite thin films

M. H. Abdel-Aziz[1,2] · A. F. Al-Hossainy[3,4] · A. Ibrahim[5] · S. A. Abd El-Maksoud[6] · M. Sh. Zoromba[1,6] · M. Bassyouni[7] · S. M. S. Abdel-Hamid[8] · A. A. I. Abd-Elmageed[9] · I. A. Elsayed[10,11] · O. M. Alqahtani[11]

Received: 18 March 2018 / Accepted: 27 July 2018 / Published online: 30 July 2018

Abstract
Carboxylic functionalized multi-walled carbon nanotubes/aniline-anthranilic acid copolymer composites with different amounts of MWCNTs were produced by the method of in situ oxidative polymerization. Thin films of the composites were fabricated by thermal evaporation method within the thickness range of 150–200 nm. The structural characteristics of the investigated composites were studied by various techniques. SEM images showed that the resulting nanoparticles have irregular entangled like-plate layers with an average diameter range of 40–60 nm. Indirect optical band gaps E_{g1} and E_{g2} were calculated depending on the energy range of composite thin films. Electronic parameters of MWCNTs/PANAA thin film, including diode ideality factor (n), series resistance (R_s) and shunt resistance (R_{sh}) were determined from the I–V characteristic in the dark under different temperatures. The values of n, R_s, and R_{sh} were found to be 3.80, 5.6×10^4 (Ω), and 1.64×10^6 (Ω), respectively at room temperature.

1 Introduction

The integration of carbon nanotubes into photovoltaic solar cells were employed as electron acceptors in combination with conjugated polymers in the organic solar cells [1, 2]. Conjugated polymers including polyaniline (PANI), polyaniline derivatives, polypyrrole, and polythiophene have good electroactivity and semiconductor properties [3–10]. They have various applications including electrochromic devices, chemical sensors, rechargeable batteries, solar cells and electrochemical applications [11–13]. The addition of CNTs into polymers in order to form composites improves the functionality of composite constituents. Using CNTs as reinforcement materials produces lightweight and strong materials. Composites of polymer/CNTs have various current applications such as antistatic packaging and electromagnetic shielding. Polymer/CNTs composites can be prepared by in situ polymerization method where the polymerization takes place in the existence of CNTs to connect physically through a

✉ M. H. Abdel-Aziz
helmy2002@gmail.com; mhmousa@alexu.eg.edu; mhmoss@kau.edu.sa

[1] Chemical and Materials Engineering Department, King Abdul-Aziz University, Rabigh 21911, Kingdom of Saudi Arabia

[2] Chemical Engineering Department, Faculty of Engineering, Alexandria University, Alexandria, Egypt

[3] Chemistry Department, Faculty of Science - New Valley, Assiut University, Assiut 71516, Egypt

[4] Chemistry Department, Faculty of Science, Northern Border University, Arar 13221, Kingdom of Saudi Arabia

[5] Physics Department, Faculty of Science, Tanta University, Tanta 31527, Egypt

[6] Chemistry Department, Faculty of Science, Port Said University, Port Said 42521, Egypt

[7] Department of Chemical Engineering, Faculty of Engineering, Port Said University, Port Said, Egypt

[8] Department of Chemical Engineering, The Egyptian Academy for Engineering and Advanced Technology, Ministry of Military Production, Cairo, Egypt

[9] Physics Department, Faculty of Science – New Valley, Assiut University, Assiut 71516, Egypt

[10] Deptartment of Physics, Faculty of Science, Damietta University, New Damietta 34517, Egypt

[11] Physics Department, Faculty of Science and Humanitarians, Prince Sattam Bin Abdulaziz University, Alkharj 11942, Kingdom of Saudi Arabia

non-covalent bond with polymers [14]. The integration of CNTs with the polymers leads to significant advances in the physical properties such as mechanical and electronic features of resulting composites [15–17]. MWCNTs/PANI composites with flexible and efficient textile electrode were early prepared and synthesis of PANI nanofibers by noncovalent interactions with CNTs were carried out by in situ polymerization methods [18, 19]. In recent years, organic polymer thin films have played a significant role in photodiodes fabrication. Photodiodes have varieties of applications such as; optical position sensors spectroscopy, optical communications, photography, beam alignment, and medical instruments. The conjugated polymer-based photovoltaic devices were developed by different scientists [20–22]. Exposing the device to photons creates excitons in depleted regions, the length of the exciton diffusion length is about 10 nm. One of the most important parameters which affect the performance of organic solar cells is the shape of the donor/acceptor interface. An interpenetrating donor/acceptor network is an ideal shape which allows fast charge separation and continuous transference paths for the created electrons through donor and acceptor molecules [23, 24]. In addition, in the polymer solar cell area, the choice of appropriate solvent is very important for the fabrication and performance of the devices [25, 26].

This study aims to prepare MWCNTs/PANAA composites based on the polymerization of aniline and anthranilic acid monomers by oxidative polymerization in the presence of MWCNTs. Thin films of MWCNTs/PANAA were prepared by thermal evaporation technique and a comprehensive experimental study of the structural, optical, magnetic and electrical properties of MWCNTs/PANAA films were carried out. The effects of both MWCNTs weight percentage and temperature on electrical transport mechanisms properties of MWCNTs/PANAA films as a heterojunction diode configuration were studied.

2 Experimental part

2.1 Materials

All substances were used without additional refinement except aniline (Aldrich). Double distillations of aniline were carried out before the polymerization process. Ortho anthranilic acid, potassium dichromate from LOBAL Chemie, and ethanol purchased from Fisher Scientific UK Limited. KNT-ICH$_{24}$,-COOH functionalized industrial, grade: multi-walled carbon nanotube, 20–40 nm diameter, 10–20 μm length, 90% carbon purity, specific surface area: 110 m^2/g, and COOH content of 1.4 wt% was used.

2.2 Preparation of MWCNTs/PANAA binary nanocomposites

Typically, five different amounts of MWCNTs-COOH, namely; 0.075, 0.22, 0.37, 0.53, and 0.78 g which is equivalent to 1, 3, 5, 7, and 10% of monomer weights respectively, were used to form the composites. Each amount of the MWCNTs was separately dispersed in 40 ml ethanol by ultrasonic homogenizer for 15 min. 2.8 ml [equivalent to 2.85 g (0.030 mol)] aniline were dispersed in 20 ml distilled water, followed by addition of drops of concentrated HCl under magnetic stirring (rpm = 500) at room temperature. 30 ml of distilled water were added to the resulting aniline salt under magnetic stirring. Separately, 4.1 g of anthranilic acid (equivalent to 0.030 mol) were dissolved in 20 ml ethanol. Anthranilic acid solution was added to aniline salt solution. The resulting MWCNTs/aniline-anthranilic acid monomers mixture was stirred by ultrasonic homogenizer for 5 min. The value of pH of the resulting mixture was adjusted at 1.5 by conc. HCl. 10 g of potassium dichromate as an oxidizing agent were dissolved in 100 ml distilled water. Dichromate solution was added to the MWCNTs/aniline-anthranilic acid monomers mixture drop by drop at room temperature under magnetic stirring (850 rpm). The resulting MWCNTs/PANAA was filtered and washed several times with distilled water, followed by washing with ethanol to get rid of the excess initiator, monomers, oligomers and then dried at 60 °C. The resulting MWCNTs/PANAA composites with weight percentages of 1, 3, 5, 7, and 10% of MWCNTs were marked by W_1, W_2, W_3, W_4 and W_5 respectively. Neat PANAA was prepared using the same steps, but without adding MWCNTs.

2.3 Fabrication of heterojunction diode of Al/MWCNTs-PANNA/Al

The heterojunction diode of Al/MWCNTs-PANNA/Al was made by the technique of thermal evaporation (Edwards type E306A, England, under a vacuum of about 10^{-4} Pa) on the surface of Al thin film. The silicon substrate was cleaned chemically and immersed in PC_4 solution (HF:HNO_3:CH_3COOH in the ratio 1:3:1) for ectching within 10 s, rinsed and cleaned with deionized water and isopropyl alcohol and then oven dried. A thick film of pure Al (100 nm) was deposited on the silicon substrate to make the bottom contact electrode as Schottky electrode. A molybdenum boat shaped filament was used to gradually heat a quartz crucible containing the MWCNTs/PANNA nanocomposite powder. Sublimation of the powder takes place during the heating process. The temperature of the substrate was kept at 503 K during the evaporation process.

A quartz crystal thickness monitor (Model TM-350 MAXTEK, Inc. USA) attached to the coating system was employed to monitor the deposition rate and the film thickness. 200 nm thickness of the MWCNTs/PANNA composite was deposited on the Al thin film. After deposition, the film thickness was also checked interferometrically by the Tolansky method [27]. Then, a top contact of mesh Al metal was deposited on the MWCNTs/PANNA layer as an Ohmic electrode which has a low contact resistance and high stability with MWCNTs/PANNA layer. A Schottky electrode has higher contact resistance than the MWCNTs/PANNA semiconductor layer. The active area of the junction was 0.39 cm^2. The schematic diagram of Al/MWCNTs–PANNA/Al heterojunction diode is presented in Fig. 1.

2.4 Characterization

The FT-IR bands of the POAP powder were obtained using a Mattson 5000 Fourier-transfrom infra red spectrometer in wave number region 400–4000 cm^{-1}. The thermal stability of the considered composites was studied by Schimadzu model 50 Thermogravemetric analyzer instrument under 10 °C/min heating rate in a nitrogen atmosphere. Crystal structure of the composites was investigated by X-ray diffractometer (RU-200BH) with 1.54 Å wave length and 12 kW maximum powr. The morphology of the composites was imaged by (SEM; Inspect S, FEI, Holland) scanning electron microscopy. Transmission electron microscope (TEM) (JEOL 100 CX II TEM 100 kV) was used to detect the shape and dimensions of the particles. The current–voltage characteristics of Al/MWCNTs-PANNA/Al heterojunction diodes were recorded in the dark by Keithley electrometer model 6517 B.

3 Results and discussion

3.1 FT-IR spectra of MWCNTs/PANAA composite powder

FT-IR bands of neat PANAA and MWCNTs/PANAA binary composites are listed in Table 1. The FT-IR spectra of MWCNTs/PANAA composites are shown in Fig. 2. The data supports the possibility of formation of binary nanocomposites in the solid phase. This stretch due to the existence of the ν(C=C) and ν(C=N) bands of benzoid and quinoid rings at 1618 and 1520 cm^{-1}. The two bands at 1231 and 1114 cm^{-1} belong to ν(C–N) of the quinoid and benzoid rings, respectively [28, 29]. The bands at 3359 and 2933 cm^{-1} can be ascribed to ν(OH) and ν(NH), respectively. The bands at 644

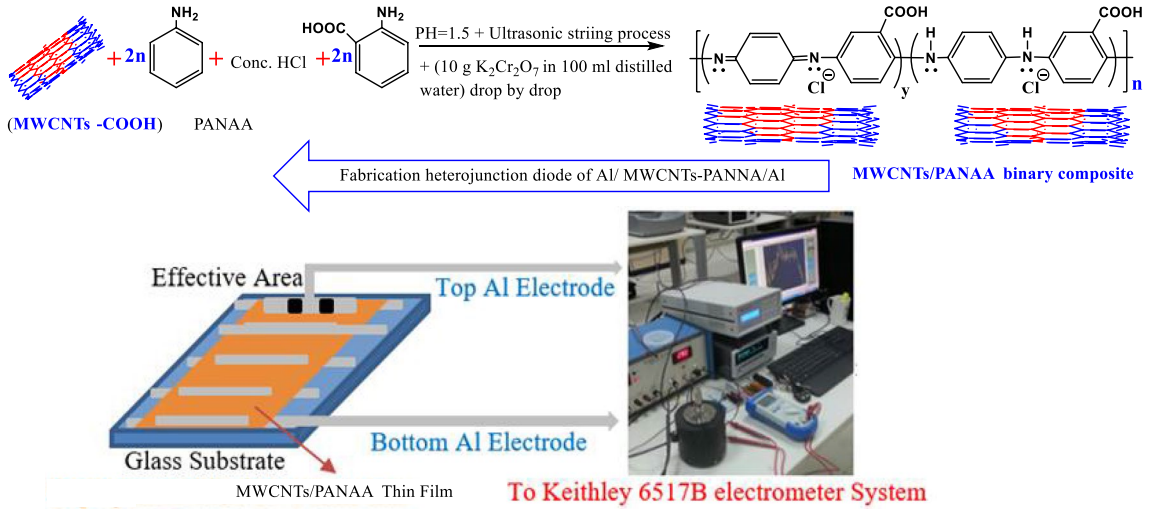

Fig. 1 The chemical structure and fabrication of MWCNTs/PANAA nanocomposites

Table 1 FTIR bands of neat PANAA and MWCNTs/PANAA composites

Compound	ν (OH), δ(OH)	ν (NH)	ν (C=C)	ν (C=N)	ν (COOH)	ν (C–N)
PANAA	3359, 975	2933	1618	1520	1440	1231, 1114
W1	3403, 949	2911	1581	1495	1309	1248, 1147
W2	3467, 954	2806	1575	1492	1297	1245, 1130
W3	3463, 947	2812	1575	1491	1298	1241, 1127
W5	3396, 954	2815	1576	1490	1375	1297, 1079

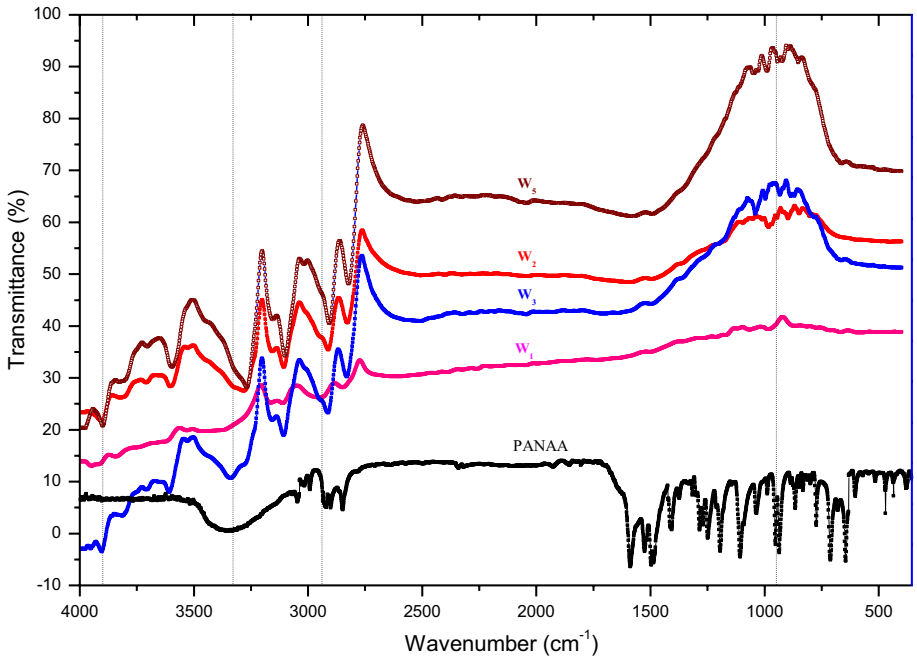

Fig. 2 FT-IR spectra of neat PANAA and MWCNTs/PANAA composites powder

and 513 cm^{-1} are corresponding to γ(COOH) and ρ(COOH) vibrations. The bonding of poly(aniline-co-anthranilic acid) (PANAA) causes distortion in the electron concentration of some active sites of the neat MWCNTs/PANAA composites. In comparison, of MWCNTs/PANAA spectra with the neat PANAA spectrum, the data show that the band at 1520 cm^{-1} which is due to ν(C=N) in the spectrum of neat PANAA was shifted to 1490 cm^{-1} in the spectrum of MWCNTs/PANAA and accompanied by a reduction in intensity. The bands at 3359 and 975 cm^{-1} which are due to ν(OH) and δ(OH) in the spectrum of PANA were shifted in the spectra of MWCNTs/PANAA (W_2–W_5) to 3403, 3467, 3463, 3396, 3402 and 949, 954, 947, 954, 952 cm^{-1}, respectively. This shift to lower wavenumber in δ(OH) suggests that both neat PANAA and MWCNTs/PANAA composites (W_2-W_5) (containing COOH group) are in bonding without shift of hydrogen ion from carboxylic group.

3.2 Thermogravimetric analysis of MWCNTs/PANAA composite powders

Figure 3 shows the TGA curves of the neat PANAA, pristine MWCNTs, and MWCNTs/PANAA composites. As displayed in Fig. 3, the pristine MWCNTs was more thermally stable and its weight decreased insignificantly with increasing temperature compared with MWCNTs/PANAA composites. The weight loss for pristine MWCNTs was 2% at 700 °C and 5% at 900 °C.

For PANAA and MWCNTs/PANAA composites the weight loss detected under 140 °C is because of dehydration, witness to that is the change of colors from pale to

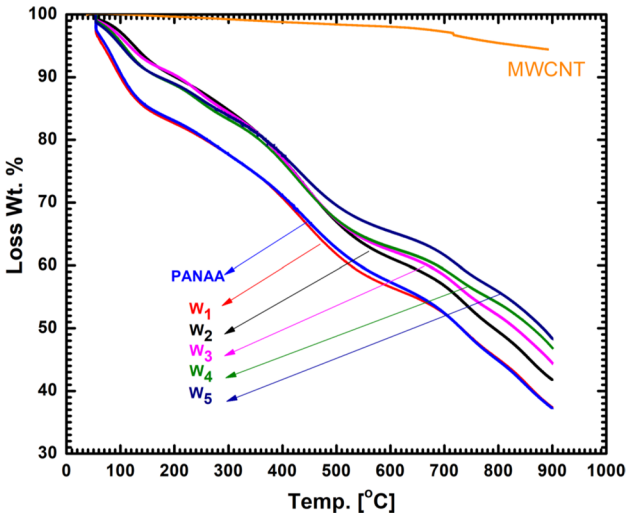

Fig. 3 TGA of neat PANAA, pristine MWCNTs and MWCNTs/PANAA composites powder

deep. This stage is an endothermic process and occurs in the temperature range from room temperature to 140 °C. After that, the thermogram of PANAA and MWCNTs/PANAA shows the weight losses within the temperature range of 140–260 °C. This corresponds to the removal of water molecules from the crystal structure of neat PANAA and MWCNTs/PANAA [30, 31]. After removal of water molecules, the decomposition process was carried out for the neat PANAA and MWCNTs/PANAA within the range of 260–500 °C through the collapse of the weakest hetero {N–C (aniline) or N–C (anthranilic acid)} bonds [32]. The last decomposition

step within the range of 500–900 °C for neat PANA and MWCNTs/PANAA composites leaves the ash, which are produced from the carbonization process under nitrogen atmosphere. The thermal stability of the PANAA increased by increasing the percentage of MWCNTs, the decomposition curve of the composites takes the same behavior of the neat PANAA curve. This can be attributed to the interaction carried out between the PANAA copolymer and MWCNTs through π-bonding with each other.

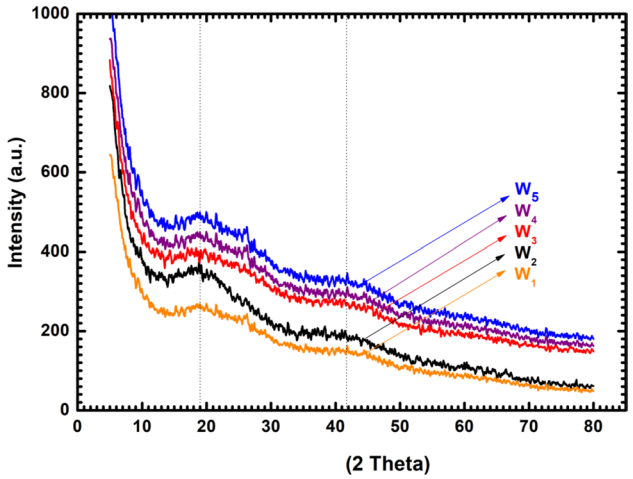

Fig. 4 XRD pattern of MWCNTs/PANAA composites powder

3.3 XRD of MWCNTs/PANAA composite powder

X-ray diffraction patterns of MWCNTs/PANAA composites with different weight percentage of MWCNTs are presented in Fig. 4. The results displayed an amorphous (no crystallinity) structure with a lack of Bragg diffraction peaks for all considered composites. The absence of peaks associated with crystalline phases and the broad halo detected in the XRD patterns confirms the amorphous structures of all the considered composites. On the other hand, the XRD pattern's intensity increases with increasing the percentage of MWCNTs.

3.4 Morphology analysis of MWCNTs/PANAA composite powder

The SEM images (Fig. 5) show that the size of the MWCNTs/PANAA composites are finely dispersed in a micorscale. The resulting particles have irregular entangled like-plate layers.

Figure 6 shows the TEM image of W_3 and W_5 nanoparticles of the as-deposited MWCNTs/PANAA composites. The

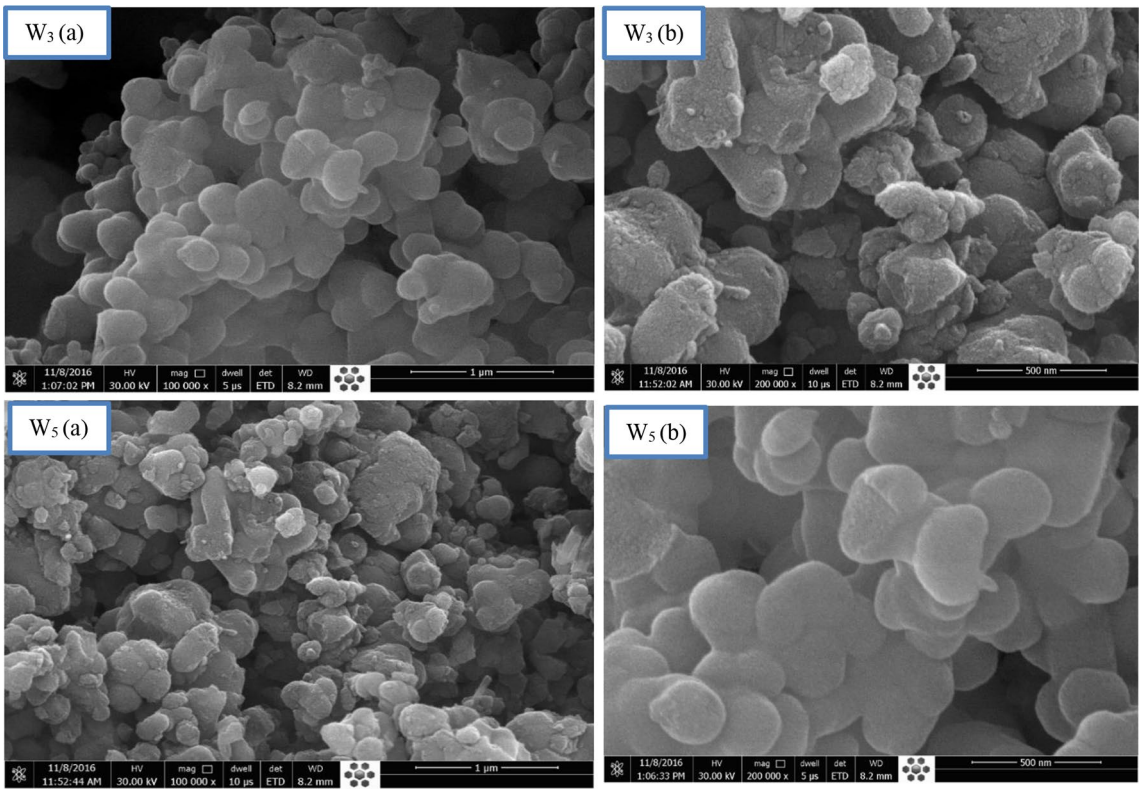

Fig. 5 Typical SEM of binary MWCNTs/PANAA composites powder (W_3 and W_5)

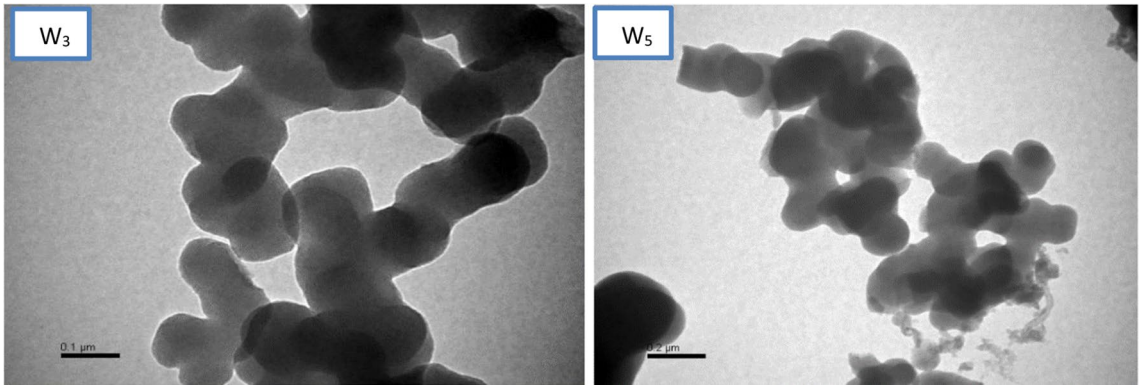

Fig. 6 TEM images of MWCNTs/PANAA composites powder with two different magnifications of W_3 and W_5

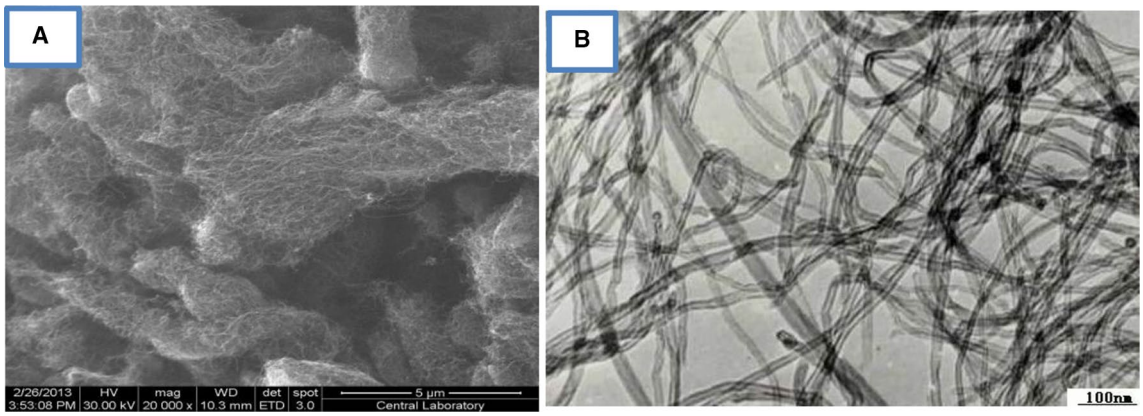

Fig. 7 SEM (**a**) and TEM (**b**) images of MWCNTs

majority of MWCNTs/PANAA particles in the composite has a length between 93.75 and 137.5 nm.

In comparison of the SEM and TEM images of MWCNTs as a blank (Fig. 7) with the prepared MWCNTs/PANAA composites, the analysis showed that the agglomerated and aggregated clusters of polymer have been formed in the composites. The deposition of the copolymer on the surface of MWCNTs converted its size from nano to microscale.

3.5 Magnetic properties of MWCNTs/PANAA composite powder

Characteristic magnetization curves for MWCNTs/PANAA nanocomposite with different percentages of MWCNTs are shown in Fig. 8. The magnetic properties of MWCNTs/PANAA binary nanocomposite were determined at room temperature using VSM (Vibrating Sample Magnetometer). Meanwhile the neat PANAA does not have magnetic properties, therefore the magnetic properties of the synthesized MWCNTs/PANAA binary nanocomposite are intensely due to the presence of MWCNTs and depend on the contents of MWCNTs in the structure. Magnetization curves

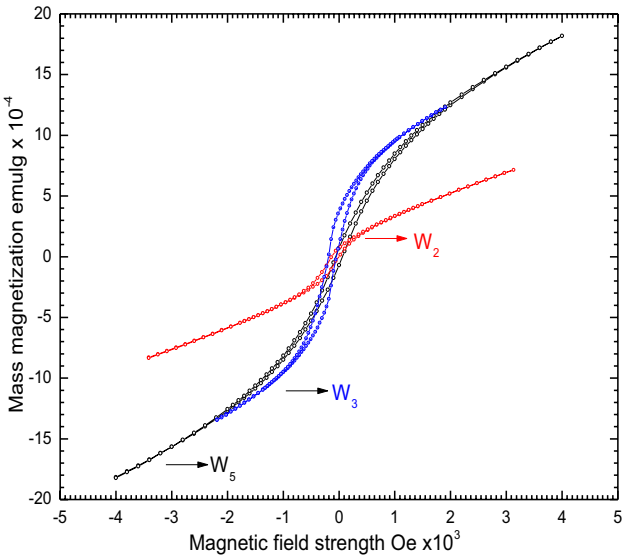

Fig. 8 Magnetization curves of MWCNTs/PANAA composites powder at room temperature

showed almost no remanence or coercivity at room temperature, signifying superparamagnetic performance by saturation magnetization values: 16.4×10^{-4}, 14.30×10^{-4} and 8.08×10^{-4} emu/g for the composites at different weight percentages of MWCNTs for W_2,W_3, and W_5 respectively. The lower values of saturation magnetization (M_s) may be ascribed to the surface effect and finite size [33, 34].

3.6 Electronic spectra and optical band gap (E_g) of MWCNTs/PANAA thin films

The UV–Vis absorption spectra of the thin film with a thickness of 200 nm from MWCNTs/PANAA were presented in Fig. 9. MWCNTs/PANAA composites give main absorption spectrum within the wavelength range of 250–1000 nm. The absorption spectra of MWCNTs/PANAA thin films are featured by two main absorption bands. The first band is located in the range of 250–410 nm. This band can be ascribed to the localized π–π* transitions [35, 36]. From the spectrum, it can be noticed that this band in the range of 250–410 nm is splitting into two peaks, one peak at 290 nm and the other one at 330 nm. The main band with the shoulder edge within the range of 500–750 nm. This can be attributed to charge transmission between the electron-rich donor and electron-deficient acceptor units within the molecules in the composites thin film. On increasing the percentage of MWCNTs, red shift takes place indicating to intermolecular interaction between the MWCNTs and PANAA [37, 38].

The spectral distribution of transmittance T (λ) and reflectance R (λ) of MWCNTs/PANAA thin films with 200 nm thickness was obtained at normal incidence within the wavelength range 200–1000 nm and shown in Fig. 10. It is clear from the data that both the spectral behavior of both T (λ) and R (λ) for the investigated films refers to the homogeneity of the films. The stability in the peak locations in the absorbing region demonstrates the stability of the structure of MWCNTs/PANAA thin film. Also the data show that at longer wavelengths (λ > 800 nm), thin film becomes transparent and light scattering is prevented (i.e., T + R = 0.80) while almost 20% is absorbed. The inequality of (T + R << 1) at smaller wavelengths (λ < 800 nm) identified as the absorbing region is due to the presence of absorption.

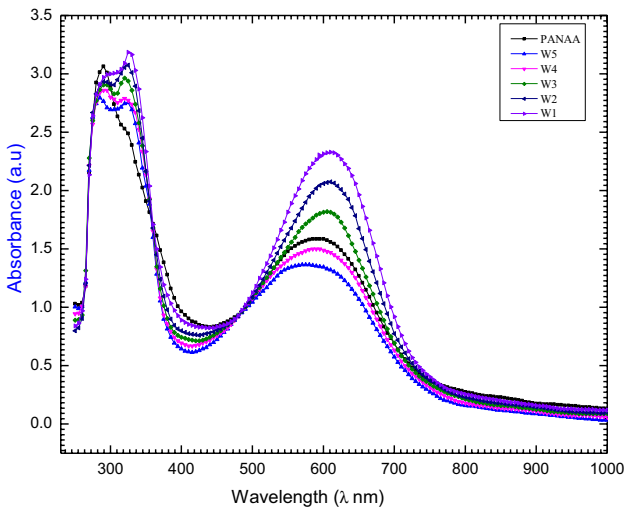

Fig. 9 The UV–Vis spectra of MWCNTs/PANAA composite thin film at room temperature

The refractive indices of optical materials are of great importance for the applications in optics devices [39]. Both refractive index ($n = ((1+R)/(1-R(\lambda))+\sqrt{(4R(\lambda)/(1-R(\lambda)^2)-k^2}$ and absorption index [$k = (\alpha\lambda/4\pi$ where α absorption coefficent)] of the resulting MWCNTs/PANAA films are depending on the percentage of transmittance and reflectance at a normal light incidence. The spectral dependencies of both n(λ) and k (λ) are presented in Fig. 11. It is clear that, both n and k are almost independent of MWCNTs percentage. At longer wave lengths the absorption index k becomes very small, indicating that the synthesized films are extremely transparent.

Estimation of the transitions' type in semiconductor materials requires analysis of optical absorption close to the absorption band boundary. The inter-band absorption coefficient (α) as a function of energy for direct permitted transition is given by [40]:

$$(\alpha h\nu)^{1/2} = B\left(h\nu - E_g\right) \tag{1}$$

where B is a characteristic constant and is a function of the transition probability, hν is the photon energy, E_g is an optical energy gap. Figure 12 depicts $(\alpha h\nu)^{0.5}$ versus photon energy for MWCNTs/PANAA thin film. The direct allowed band gap (E_g) for the film is estimated from the x-axis intercepts at $(\alpha h\nu)^{0.5} = 0$. Two allowed direct optical band gaps E_{g1} and E_{g2} were gotten depending on the range of photon energy and are listed in Table 2 for MWCNTs/PANAA binary polymer films.

The complex optical conductivity ($\sigma^* = \sigma_1(\lambda) + i\sigma_2(\lambda)$) is correlated to the complex dielectric constant ($\varepsilon^* = \varepsilon_1(\lambda) + i\varepsilon_2(\lambda)$) by the relation [41–43]:

$$\sigma_1 = \omega\epsilon_2\epsilon_0 \tag{2}$$

and

$$\sigma_2 = \omega\epsilon_1\epsilon_0 \tag{3}$$

where

$$\epsilon_1 = n^2 - k^2 \tag{4}$$

and

$$\epsilon_2 = 2nk \tag{5}$$

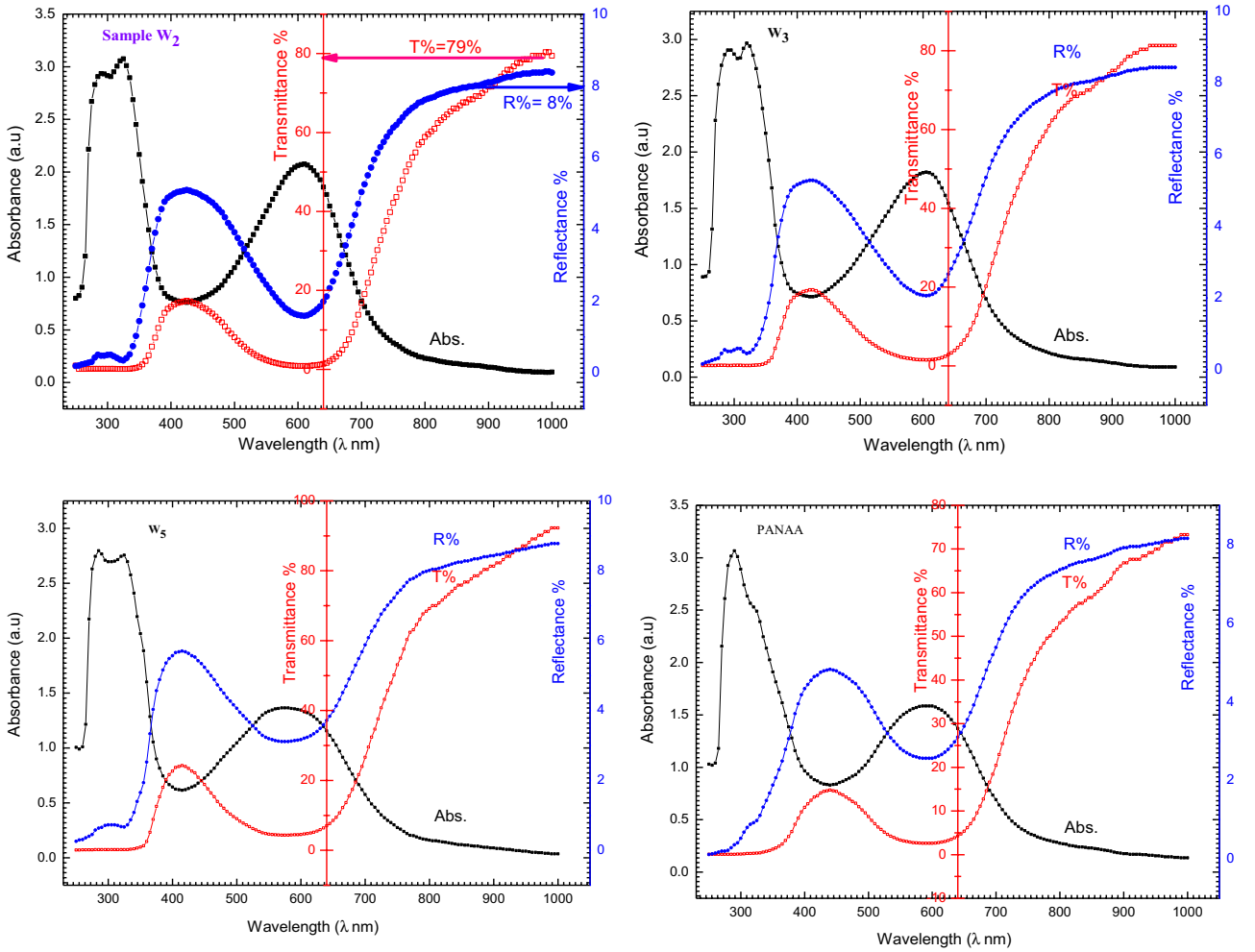

Fig. 10 The transmittance T (λ) and the reflectance R (λ) of MWCNTs/PANAA composite thin films

The real σ_1 and imaginary σ_2 parts of the optical conductivity vs. photon energy are shown in Fig. 13. From the figure, it can be noticed that on increasing the photon energy σ_1 decreases and σ_2 increases. The values of E_g have the range 1.75–2.6 and 3.5 eV, theses values obtained at the points of intersections between σ_1 and σ_2.

3.7 Electrical properties of MWCNTs/PANAA thin films

The typical forward bias voltage (V) and current (I) characteristics under different temperatures obtained from MWCNTs/PANAA film are presented in Fig. 14. The obtained forward current increases with increasing the MWCNTs percentage. The forward bias, I–V features of the examined films might be diverged significantly from linearity at the higher voltage region. For a non-ideal heterojunction diode which include series resistance effect the I–V correlation is stated as [44]:

$$I = A\,A^{*}\,T^{2}\,exp^{\left(-\frac{q\varphi_B}{k_BT}\right)}\left[exp^{\left(\frac{q(V-IR_s)}{nk_BT}\right)}\right] \tag{6}$$

where A is the contact area, A* is the Richardson constant, φ_B is the barrier height, T is the absolute temperature, q is the electron charge and k_B is the Boltzmann constant. One of the most important factors affecting on the dark forward I–V curves is the series resistance (R_s). Since, R_s is affected by the existence of the expected interface layer among the copolymers and leads to non-ideal performance. The R_s decrease the distance of the linear behavior in the forward features of the fabricated sample. The value of R_s can be estimated using the method established by Cheung formula [45]:

$$\frac{dV}{d\ln(I)} = n\frac{k_BT}{q} + R_s\,I \tag{7}$$

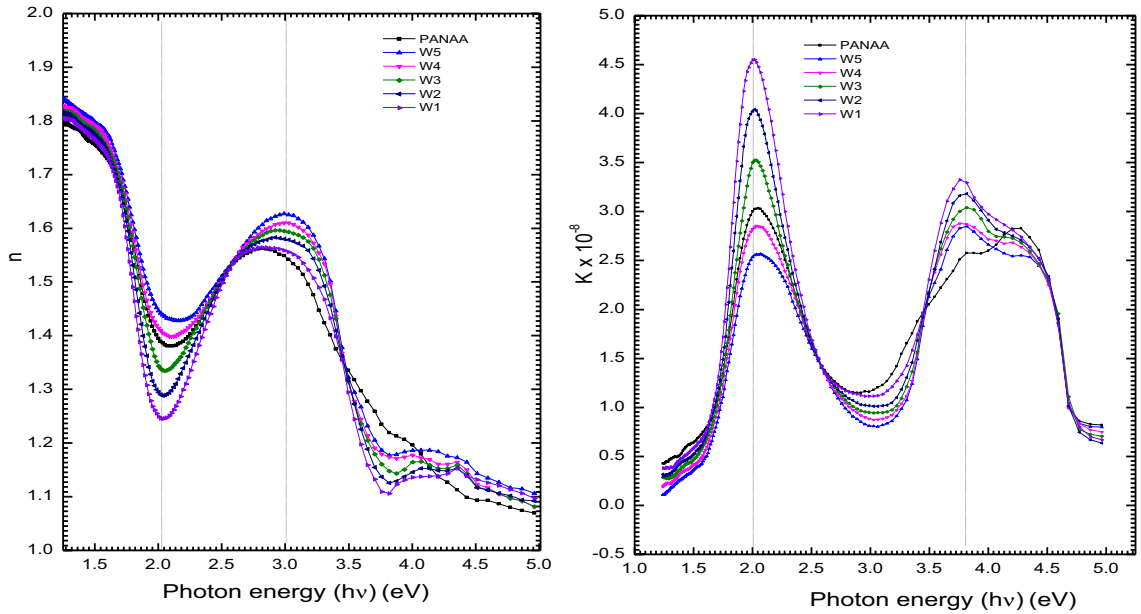

Fig. 11 Dispersion of the refractive index n and the absorption index k of MWCNTs/PANAA composite thin films

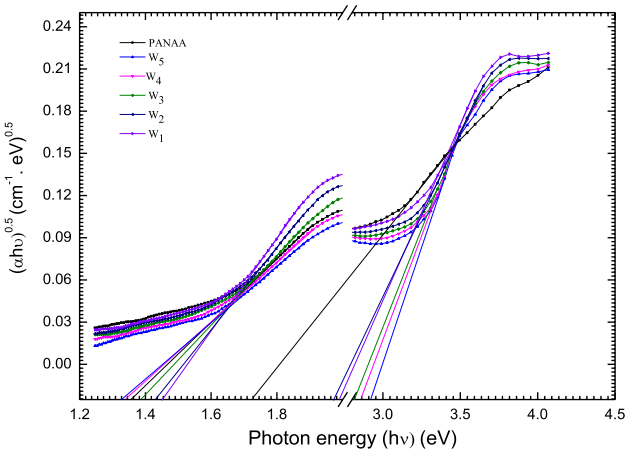

Fig. 12 Photon energy dependence of $(\alpha h)^{0.5}$ for MWCNTs/PANAA composite thin film

Table 2 Values of onset energy gap and fundamental energy gap, for MWCNTs/PANAA binary polymers thin film

Sample MWCNTs/PANAA	Onset energy gap (eV) E_{g1}	Fundamental energy gap (eV) E_{g2}
W_1	1.46	2.81
W_2	1.44	2.60
W_3	1.38	2.21
W_4	1.34	2.63
W_5	1.32	2.83
Neat PANAA	1.36	2.19

Equation (7) states that a plot of $\frac{dV}{d\ \ln(I)}$ versus I gives a straight line (for the data in the downward curved region of the forward bias I–V characteristics). The slope of the line gives R_s and n can be obtained from the y-axis intercept $\left(n\frac{k_BT}{q}\right)$ for MWCNTs/PANAA composite (W_5) at different temperatures (Fig. 15). The obtained values of the ideality factor n, and R_s for MWCNTs/PANAA composite (W_5) at different temperatures are recorded in Table 3. From the table it is clear that the values of both n and Rs are strongly dependent on temperature. It is noted that, there is a continuous decrease in the diode ideality factor n with increasing temperature. On the other hand, R_s values are inversely proportional to temperature. Existence of recombination charges, and aggregation of primary and secondary particles during polymerization are possible causes which make the values of $n > 1$ [46].

The junction resistance R_j for the fabricated MWCNTs/PANAA composite film is expressed as $R_j = \partial V/\partial I$. At upper voltages, R_j value reaches a constant value called series resistance R_s. However, at higher reverse voltages, the R_j value has a constant value termed shunt resistance R_{sh} [47, 48]. The R_s and R_{sh} values were calculated from the curve of R_j –V plotted and were listed in Table 3.

At higher voltages, I–V characteristic of MWCNTs/PANAA composite film is affected by MWCNTs transport properties as a semiconductor material [49]. For this reason, the current–voltage characteristics of the diode were plotted as displayed in Fig. 16 (ln (I) vs. ln (V)). The I–V curve was analyzed via $I \propto V^m$ relation. The average value of

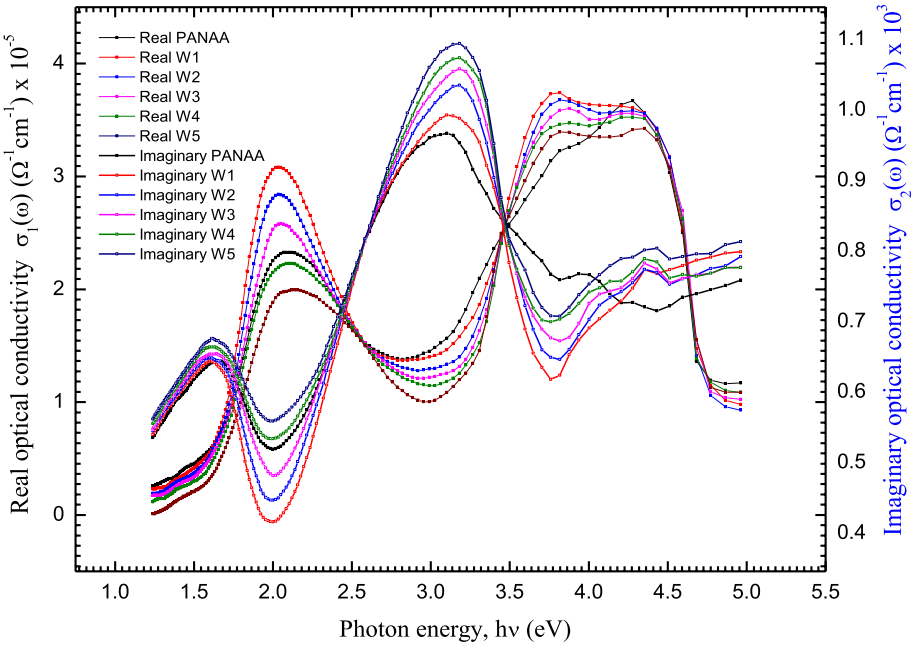

Fig. 13 The dependence of the real and imaginary parts of the optical conductivity on the photon energy hν for MWCNTs/PANAA composite thin films

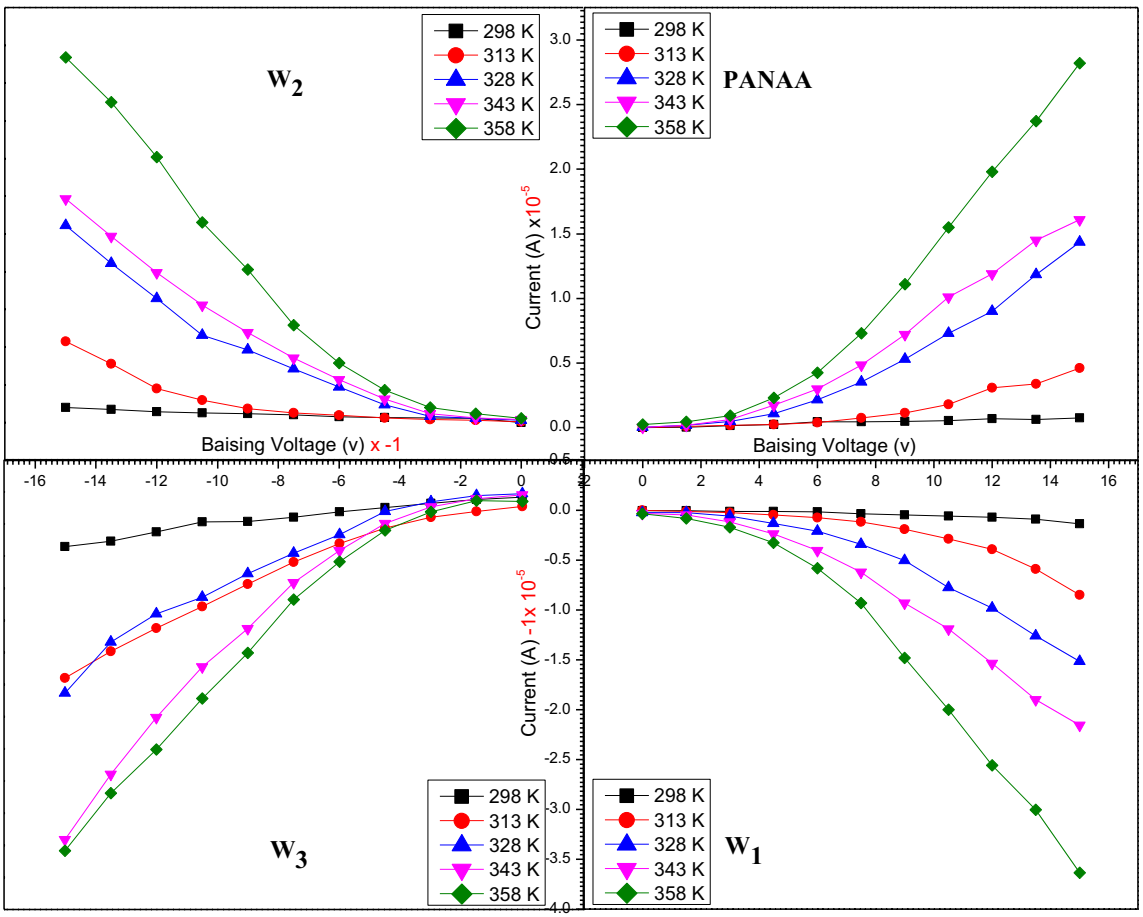

Fig. 14 Forward current–voltage characteristics of the MWCNTs/PANAA composite thin film at room temperature

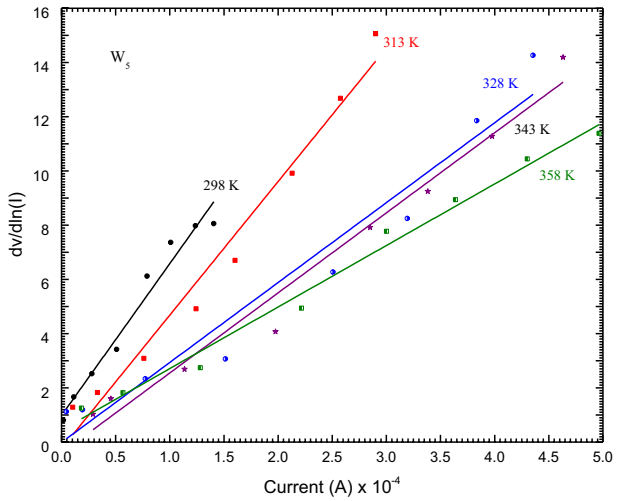

Fig. 15 Plots of dV/d ln(I)–I of the MWCNTs/PANAA composite (W_5) thin films under different temperature

Table 3 I–V characteristic parameters of the MWCNTs/PANAA films (W_5)

Temperature K	Ideality factor (n)	Series resistance $R_s \times 10^4$	Shunt resistance $R_{Sh} \times 10^5$
298	3.807	5.60	1.64
313	2.67	4.91	1.39
328	2.49	2.97	1.10
343	1.338	2.93	1.00
358	1.812	2.25	0.80

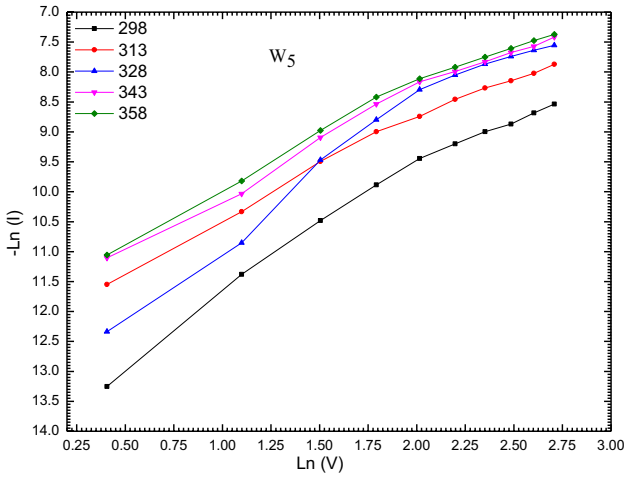

Fig. 16 Plot of Ln *I*–Ln *V* of MWCNTs/PANAA composite (W_5) thin films

Table 4 Values of I–V characteristic parameters of the MWCNTs/PANAA films

Temperature K (room temperature)	n	$R_s \times 10^4$	$R_{Sh} \times 10^5$	References
MWCNTs/PANAA composite (W_5) thin films	3.807	5.60	1.64	This work
Au/n-PANA-ES/p-Si/Al solar cell device	3.229	0.099	4.60	[52]
Ag/PANI/n-type Si	4.59	3.41	–	[53]
A poly(3-hexylthiophene) (P3HT):1-(3-methoxycarbonyl) propyl-1-phenyl-[6,6]-methano fullerene (PC61BM)	1.60	5.11	1.3	[54]

m is 1.7, whereas the temperature increased the value of m decreases, this may be attributed to the decreases of the R_s with temperature. This recommends that most of the traps are occupied and participation of free carrier to electric field becomes noteworthy [50, 51].

The values of the obtained I–V characteristic parameters of the MWCNTs/PANAA films in in comparison with other compounds [52–54] are listed in Table 4. These results demonstrate that the MWCNTs/PANAA films as a conjugated conductor nanocomposite polymers are reliable for application in real optoelectronic devices.

4 Conclusions

The structural, optical parameters and the electrical properties have been studied for MWCNTs/PANAA composite thin films. XRD and SEM results indicate that MWCNTs/PANAA composite thin films have an amorphous structure with a particle size 40–60 nm.

Magnetization properties showed that there are almost no remanence or coercivity at room temperature taking super paramagnetic behavior. MWCNTs/PANAA composite films have about 75% of transmittance in the visible range.

The band gap of MWCNTs/PANAA composite thin films was determined by real and imaginary optical conductivity and was found in a good agreement with the Tauc band gap. The estimated average values of the onset and fundamental energy gaps, for MWCNTs/PANAA binary polymers thin film are (1.46–1.32 eV) and (2.81–2.83 eV) depending on the MWCNT weight percentage. The diode ideality factor, series resistance R_s, and shunt resistance R_{sh} values determined from I–V–T curves in the dark condition for the MWCNTs/PANAA composite thin films and were found to be (3.807–1.812), (5.6–2.25 × 10^4 Ω)and (1.64–0.8 × 10^5 Ω), respectively. The nanostructures MWCNT/PANAA thin films have high transparency and a good electrical properties for application in solar cells and optoelectronics.

References

1. E. Kymakis, G.A. Amaratunga, Carbon nanotubes as electron acceptors in polymeric photovoltaics. Rev. Adv. Mater. Sci. **10**, 300–305 (2005)
2. R.L. Patyk, B.S. Lomba, A.F. Nogueira, C.A. Furtado, A.P. Santos, R.M.Q. Mello, L. Micaroni, I.A. Hümmelgen, Carbon nanotube–polybithiophene photovoltaic devices with high open-circuit voltage. Physica Status Solidi (RRL)-Rapid Res. Lett. **1**, R43 – R45 (2007)
3. M. Sh. Zoromba, M.H. Abdel-Aziz, Ecofriendly method to synthesize poly (o-aminophenol) based on solid State polymerization and fabrication of nanostructured semiconductor thin film. Polymer **120**, 20–29 (2017)
4. M. Pandey, S. Sadakata, S. Nagamatsu, S.S. Pandey, S. Hayase, W. Takashima, Layer-by-layer coating of oriented conjugated polymer films towards anisotropic electronics. Synth. Met. **227**, 29–36 (2017)
5. H. Hongchao, C. Yingde, Synthesis and conductive properties of a novel azobenzene-based conjugated polymer. Synth. Met. **205**, 106–111 (2015)
6. M. Sh Zoromba, M.I.M. Ismail, M. Bassyouni, M.H. Abdel-Aziz, N. Salah, A. Alshahrie, A. Memic, Fabrication and characterization of poly (aniline-co-o-anthranilic acid)/magnetite nanocomposites and their application in wastewater treatment. Colloids Surf. A **520**, 121–130 (2017)
7. X. Wang, Q. Su, Y. Li, C. Cheng, Y. Xia, L. He, H. Li, G. Shu, F. Wang, Synthesis and photovoltaic properties of donor–acceptor conjugated polymers based on 4, 7-dithienyl-2, 1, 3-benzothiadiazole functionalized silole. Synth. Met. **220**, 433–439 (2016)
8. M. Sh. Zoromba, A.A.M. Belal, A.E.M. Ali, F.M. Helaly, A.S. Badran, A.A. Abd El-Hakim, Preparation and characterization of some NR and SBR formulations containing different modified kaolinite. Polym-Plast Technol Eng **46**, 1–7 (2007)
9. M. Sh. Zoromba, S. Alghool, S.M.S. Abdel-Hamid, M. Bassyouni, M.H. Abdel-Aziz, Polymerization of aniline derivatives by $K_2Cr_2O_7$ and production of Cr_2O_3 nanoparticles. Polym. Adv. Technol. **28**, 842–848 (2017)
10. N.M. Hosny, N. Nowesser, A.S. Al-Hussaini, M. Sh. Zoromba, Doped copolymer of polyanthranilic acid and o-aminophenol (AA-co-OAP): synthesis, spectral characterization and the use of the doped copolymer as precursor of α-Fe_2O_3 nanoparticles. J. Mol. Struct. **1106**, 479–484 (2016)
11. S. Guenes, H. Neugebauer, N.S. Sariciftci, Conjugated polymer-based organic solar cells. Chem. Rev. **107**, 1324–1338 (2007)
12. M.H. Abdel-Aziz, I. Nirdosh, G.H. Sedahmed, Liquid–solid mass and heat transfer behavior of a concentric tube airlift reactor. Int. J. Heat Mass Transf. **58**, 735–739 (2013)
13. G.H. Sedahmed, Y.A. El-Taweel, A.H. Konsowa, M.H. Abdel-Aziz, Mass transfer intensification in an annular electrochemical reactor by an inert fixed bed under various hydrodynamic conditions. Chem. Eng. Process. **50**, 1122–1127 (2011)
14. B. Dörling, S. Sandoval, P. Kankla, A. Fuertes, G. Tobias, M. Campoy-Quiles, Exploring different doping mechanisms in thermoelectric polymer/carbon nanotube composites. Synth. Met. **225**, 70–75 (2017)
15. L.-B. Kong, J. Zhang, J.-J. An, Y.-C. Luo, L. Kang, MWNTs/PANI composite materials prepared by in-situ chemical oxidative polymerization for supercapacitor electrode. J. Mater. Sci. **43**, 3664–3669 (2008)
16. M. Bassyouni, S.A. Gutub, U. Javaid, M. Awais, S. Rehman, S.M.-S. Abdel Hamid, M.H. Abdel-Aziz, A. Abouel-Kasem, H. Shafeek, Assessment and analysis of wind power resource using weibull parameters. Energy Explor. Exploit. **33**, 105–122 (2015)
17. N. Iqbal, S. Sagar, M.B. Khan, M.I. Bassyouni, Z.M. Khan, Aluminum silicate fibers impregnateacrylonitrile butadiene rubber composites: ablation, thermal transport/stability, and mechanical inspection. J. Appl. Polym. Sci. **130**, 4392–4400 (2013)
18. N. Wang, Y. Wang, Z. Yu, G. Li, In situ preparation of reinforced polyimide nanocomposites with the noncovalently dispersed and matrix compatible MWCNTs. Compos. A **78**, 341–349 (2015)
19. P. Jimenez, W.K. Maser, P. Castell, M.T. Martinez, A.M. Benito, Nanofibrilar polyaniline: direct route to carbon nanotube water dispersions of high concentration. Macromol. Rapid Commun. **30**, 418–422 (2009)
20. A. Ibrahim, A.F. Al-Hossainy, Thickness dependence of structural and optical properties of novel 2-((1,1-bis(diphenylphosphino)-2-phenylpropan-2-yl)-chromium tetracarbonyl-amino)-3-phenyl propanoic acid copper (II) (DPP-Cr- Palan-Cu) nanocrystalline thin film. Synth. Met. **209**, 389–398 (2015)
21. W. Feng, A. Fujii, S. Lee, H. Wu, K. Yoshino, Broad spectral sensitization of organic photovoltaic heterojunction device by perylene and C6. J. Appl. Phys. **88**, 7120–7123 (2000)
22. A.A. Al-Ghamdi, F. El-Tantawy, New electromagnetic wave shielding effectiveness at microwave frequency of polyvinyl chloride reinforced graphite/copper nanoparticles. Compos. A **41**, 1693–1701 (2010)
23. P. Peumans, A. Yakimov, S.R. Forrest, Small molecular weight organic thin-film photodetectors and solar cells. J. Appl. Phys. **93**, 3693–3723 (2003)
24. S.R. Forrest, The path to ubiquitous and low-cost organic electronic appliances on plastic. Nature **428**, 911–918 (2004)
25. S.E. Shasheen, C.J. Brabec, N.S. Sariciftci, F. Padinger, T. Fromherz, J.C. Hummelen, 2.5% efficient organic plastic solar cells. Appl. Phys. Lett. **78**, 841–843 (2001)
26. T. Martens, T. Munters, L. Goris, J. D'Haen, K. Schoupeduen, M. D'Olieslaeger, L. Lusten, D. Vanderzende, W. Greens, J. Poortmans, L. De Schepper, J.V. Mance, Nanostructured organic *pn* junctions towards 3D photovoltaics. Appl. Phys. A **79**, 27–30 (2004)
27. S. Tolansky, *Multiple-Beam Interference Microscopy of Metals* (Academic Press, London, 1970), p. 55
28. I.M. Awad, F.S. Hassan, A.E. Mohamed, A.F. Al-Hossainy, Diphosphine compounds: part I. Novel biologically active 1,1′bis-AND/OR 1,2-cis-(diphenylphosphino-) ethene and their complexes [M (CO) n {Ph_2P (CHn) nPPh2}] & [Cu (Cl)$_2$ {Ph2P (CHn) nPPh_2}],(M = W, Mo, Cr_n= 1, 2… n). Phosphorus Sulfur Silicon **179**, 1251–1266 (2004).
29. F.S. Hassan, A.F. Al-Hossainy, A.E. Mohamed, D. Compounds, Part III: UV/visible spectroscopy and novel routes to functionalized diphosphine-M (CO) 6 complexes (M = W, Mo, or Cr). Phosphorus Sulfur Silicon, **184**, 2996–3022 (2009)
30. N. Hosny, M. Sh. Zoromba, G. Samir, S. Alghool, Synthesis, structural and optical properties of Eskolaite nanoparticles derived from Cr doped polyanthranilic acid (CrPANA). J. Mol. Struct. **1122**, 117–122 (2016)
31. N.A. Anaan, E.M. Saad, S.M. Hassan, I.S. Butler, S.I. Mostafa, Preparation, characterization and pH-metric measurements of 4-hydroxysalicylidenechitosan Schiff-base complexes of Fe(III), Co(II), Ni(II), Cu(II), Zn(II), Ru(III), Rh(III), Pd(II) and Au(III). Carbohydr. Res. **346**, 775–793 (2011)
32. A.F. Al-Hossainy, A. Ibrahim, Synthesis, structural and optical properties of novel3-(3,5-dimethyl-1Hpyrazol-1-yl)-1-(diphenylphosphino)-2-((diphenylphos-phino)methyl)-3-methyl butanone-1,2-diphenylethane-1,2-diaminetungsten dicarbonyl (PyrPMB-W) nanostructure thin film. Opt. Mater. **46**, 131–140 (2015)
33. S. El-Sayed, B. Jean, Synthesis, structural characterization and anticancer activity of some new complexes of 6-amino-4-hydroxy-2-thiopyrimidine. J. Mol. Struct. **1028**, 208–214 (2012)

34. K.S. Akamatsu, M. Fujii, T. Tsuruoka, S. Nakano, T. Murashima, H. Nawafune, Mechanistic study on microstructural tuning of metal nanoparticle/polymer composite thin layers: hydrogenation and decomposition of polyimide matrices catalyzed by embedded nickel nanoparticles. J. Phys. Chem. C **116**, 17947–17954 (2012)
35. J.M.D. Coey, A.H. Morrish, G.A. Sawatzky, A Mossbauer study of conduction in magnetite, J. de Physique **32**, C1.271–C1.273 (1971)
36. A.F. Al-Hossainy, Synthesis, spectral, thermal, optical dispersion and dielectric properties of nanocrystalline dimer complex (PEPyr–diCd) thin films as novel organic semiconductor. Bull. Mater. Sci. **39**, 209–222 (2016)
37. O.A. El-Gammal, A.F. Al-Hossainy, S.A. El-Brashy, Spectroscopic, DFT, optical band gap, powder X-ray diffraction and bleomycin-dependant DNA studies of Co (II), Ni (II) and Cu (II) complexes derived from macrocyclic Schiff base. J. Mol. Struct. **1165**, 177–195 (2018)
38. M.S. Zoromba, A. Al-Hossainy, M. Abdel-Aziz, Conductive thin films based on poly (aniline-co-o-anthranilic acid)/magnetite nanocomposite for photovoltaic applications. Synth. Met. **231**, 34–43 (2017)
39. A.M. Badr, A.A. El-Amin, A.F. Al-Hossainy, Elucidation of charge transport and optical parameters in the newly 1CR-dppm organic crystalline semiconductors. J. Phys. Chem. C **112**, 14188–14195 (2008)
40. A.M. Badr, A.A. EL-Amin, A.F. Al-Hossainy, Synthesis and optical properties for crystals of a novel organic semiconductor [Ni $(Cl)_2\{(Ph_2P)_2CHC(R_1R_2)NHNH_2\}$]. Eur Phys. J B **53**, 439–448 (2006)
41. S.H. Gee, Y.K. Hong, D.W. Erickson, M.H. Park, Synthesis and aging effect of spherical magnetite (Fe_3O_4) nanoparticles for biosensor applications. J. Appl. Phys. **93**, 7560–7562 (2003)
42. M. Fox, O.M. Ser, Condens. Matter Phys. **64**, 76–78 (2001)
43. G.B. Sakr, I.S. Yahia, M. Fadel, S.S. Fouad, N. Romcevic, Optical spectroscopy, optical conductivity, dielectric properties and new methods for determining the gap states of CuSe thin films. J. Alloys Compd. **507**, 557–562 (2010)
44. M.Y. Han, H. Huang, C.H. Chew, L.M. Gan, X.J. Zhang, W. Ji, Large nonlinear absorption in coated Ag_2S/CdS nanoparticles by inverse microemulsion. J. Phys. Chem. B **102**, 1884–1887 (1998)
45. S. Aydogan, M. Saglam, A. T¨urut, On the some electrical properties of the non-ideal PPy/p-Si/Al structure. Polymer **46**, 10982–10988 (2005)
46. F. Yakuphanoglu, M. Sekerci, O.F. Ozturk, The determination of the optical constants of Cu(II) compound having 1-chloro-2,3-*o*-cyclohexylidinepropane thin film. Opt. Commun. **239**, 275–280 (2004)
47. S.K. Cheung, N.W. Cheung, Extraction of Schottky diode parameters from forward current-voltage characteristics. Appl. Phys. Lett. **49**, 85–87 (1986)
48. S. Angappane, N. Rajeev Kimi, T.S. Natarajan, G. Rangarajan, B. Wessling, Pani-PMMA lend/metal Schottly barriers. Thin Solid Films **417**, 202–205 (2002)
49. A.S. Darwish, A.S. Riad, H.S. Soliman, Electrical conductivity and the effect of temperature on photoconduction of n-ZnSe/p-Si rectifying heterojunction cells. Semicond. Sci. Technol. **11**, 96 (1995)
50. M.M. El-Nahass, K.F. Abd-El-Rahman, A.A.A. Darwish, Fabrication and electrical characterization of p-NiPc/n-Si heterojunction. Microelectron. J. **38**, 91–95 (2007)
51. A.K. Mukherjee, R. Menon, Role of mesoscopic morphology in charge transport of doped polyaniline. Pramana **58**, 233–239 (2002)
52. A.F. Al-Hossainy, H.K. Thabet, M. Sh. Zoromba, A. Ibrahim, Facile synthesis and fabrication of a poly (ortho-anthranilic acid) emeraldine salt thin film for solar cell applications. New J. Chem. **42**, 10386–10395 (2018)
53. F. Yakuphanoglu, E. Basaran, B. Şenkal, E. Sezer, Electrical and optical properties of an organic semiconductor based on polyaniline prepared by emulsion polymerization and fabrication of Ag/polyaniline/n-Si Schottky diode. J. Phys. Chem. B **110**, 16908–16913 (2006)
54. T. Kirchartz, F. Deledalle, P.S. Tuladhar, J.R. Durrant, J. Nelson, On the differences between dark and light ideality factor in polymer: fullerene solar cells. J. Phys. Chem. Lett. **4**, 2371–2376 (2013)